BROSS Technical Background

Written by Claire Beveridge of University of Washington SASWE Research Group.

Originally published on 29 April 2020

1. Introduction

BROSS ("Bangladesh Remote Sensing of Suspended Sediments") is a tool developed for the Bangladesh Water Development Board (BWDB) by the University of Washington SASWE Research Group. BROSS provides spatially and temporally distributed suspended sediment concentration (SSC) predictions for the Brahmaputra-Jamuna, Ganges-Padma, and Padma rivers of Bangladesh (Figure 1). BROSS uses satellite data as inputs to SSC models calibrated for Bangladesh rivers. BROSS is not intended to replace any existing approaches of BWDB for sediment monitoring and management, but there is substantial opportunity for it to complement and provide another layer of information to aid in decision-making.

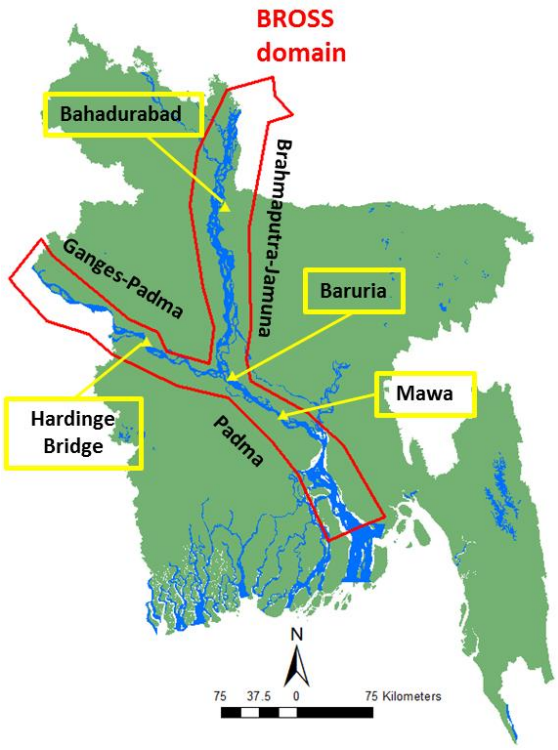

FIGURE 1: Bangladesh major rivers and BROSS domain. Yellow triangles are in situ monitoring points. *Data layers source: https://data.humdata.org/. Map produced in ArcGIS.*

This manual provides technical background on BROSS. In the text that follows, Section 2 provides background theory on satellite remote sensing of sediment. Section 3 describes the data used in implementing and operating BROSS. Section 4 describes how BROSS was calibrated. Section 5 discusses calibration results. Section 6 discusses limitations and uncertainty of BROSS outputs. Section 7 provides suggestions for future work and conclusion.

Information on how to operate BROSS are found in the accompanying user manuals (Beveridge, 2020 and Beveridge and Ahmad, 2020). Further details on the stakeholder engagement in developing BROSS will be found in a forthcoming journal publication (Beveridge et al., forthcoming)

2. Background theory on satellite remote sensing of sediment

Satellite remote sensing offers a practical response to the sustainable sediment monitoring and management needs. Satellite remote sensing provides extensive spatial coverage, frequent and extensive temporal records, cost-effectiveness, and readily transferable data and methods. Satellite remote sensing has been broadly applied in literature for monitoring SSC of water bodies due to the relationship between SSC and satellite remote sensing visible (red, green, blue) and near infrared (NIR) bands (e.g., Ritchie et al., 1987; Pavelsky & Smith, 2009; Zhang et al., 2014; Gholizadeh et al., 2016; Yepez et al., 2018). Essentially, higher levels of suspended sediment increase visible and NIR surface reflectance due to the backscattering effect of sediment in the water column (Peterson et al., 2018; Ritchie et al., 2003).

Approaches for estimating SSC from satellite remote sensing are generally either empirical or physics-based (Wackerman et al., 2017). In developing BROSS, we used two empirical approaches since there is insufficient Bangladesh river sediment data available to properly parametrize physics-based models. One empirical approach was a regression between in situ SSC and remote sensing visible and NIR data. We used regression because of its simplicity and widespread application. A second approach was the machine learning technique of artificial neural networks (ANN), which is more advanced and has been found to be stronger than traditional regression techniques (Peterson et al., 2018). We used ANN because it is well-suited for the highly complicated nature of Bangladesh rivers.

2.1. Regression

Linear regression techniques for estimating SSC have commonly used the visible (red, green, blue) and NIR bands of the Landsat satellite series (TM, ETM+, OLI) to correlate to in situ SSC measurements (Gholizadeh et al., 2016). Generally, regression has been conducted between in situ measurements and a single band or band ratio, with the values in linear or exponential form. The red band (alone or in a ratio) has been used most often. Using band ratios has been more robust than using single bands, particularly when sediment color varies (Pavelsky and Smith, 2009). Regression relationships have typically been exponential, linear, or 2nd order polynomial (higher order polynomials often overfit). Exponential relationships have often been strongest, particularly for high SSC (>50 mg/L) (Pavelsky and Smith, 2009; Wackerman et al., 2017).

The only previous study we found that used regression to predict SSC from surface reflectance in Bangaldesh inland waters was by Islam et al. (2001). They used four data points from Bahadurabad and Hardinge Bridge in situ monitoring points that were collected in year 1991, and one data point from a different river system. They found a linear relationship using the red band to be optimal. However, when we tested the relationship developed by Islam et al. (2001) we found that the range of predicted values was low compared to the range of observed SSC values. This is likely because of the low number of data points used in the calibration.

2.2. Artificial Neural Networks (ANN)

ANN uses pattern recognition. ANN models can capture both linear and non-linear relationships and are generally found to be superior to and more flexible than regression techniques (Peterson et al., 2018; Sudheer et al, 2006). Although relatively few studies have applied ANN techniques to remote sensing of river suspended sediment, the results are promising (Peterson et al., 2018). However, because of the complexity of ANN models, the end-user typically does not know how the model is working and why the results may be a certain way (e.g., it is a “black box”). It is important that those who are developing ANN models understand the theoretical foundation and ANN modeling approaches (see Maier and Dandy, 2000; Loy, 2019)

ANNs consist of several layers with interconnected nodes and are highly customizable. The most common form of an ANN model is the “feedforward neural network” in which model information is passed forward through nodes, not looped. Information is first passed to the model

input layer and then through a series of hidden layers. Each layer has a specified dimensionality, taking in a set of weighted inputs and generating outputs based on a specified activation function. The weights are developed based on the calibration data (Maier and Dandy, 2000; Loy, 2019).

Developing a predictive ANN model consists of several stages and decisions. Following the logic used in developing regression models, ANN inputs should be those that have a strong correlation with SSC. Hence, individual bands and band ratios can be inputs along with other band combinations (e.g., total visible reflectance; red/green + NIR). Other spatial (e.g., sample monitoring station) and temporal (e.g., sample month) information can also be inputs.

3. Data

3.1. In situ data

There are four in situ monitoring points along the main stem rivers for which suspended sediment and streamflow discharge data is collected by BWDB (Figure 1): Bahadurabad (Brahmaputra-Jamuna river), Hardinge Bridge (Ganges-Padma river), Baruria (Padma river) and Mawa (Padma river). Suspended sediment data is typically collected by BWDB using a Binkley silt sampler. A river cross-section is divided into approximately 25 sub-sections such that the streamflow in each section is not higher than 10% of the total cross-section streamflow. Then, suspended sediment samples are collected in each sub-section at alternating depths of 0.2D and 0.8D, where D is the total sub-section depth. The total suspended sediment discharge is then determined using all sub-section samples (personal communication, Dr. Robin Biswas, September 19, 2019).

We were provided with the complete suspended sediment discharge, Q_s (units of kilograms per second [kg/s]), and streamflow discharge, Q (units of cubic meters per second, [m^3/s]), datasets for these four in in situ monitoring points. The suspended sediment discharge data was provided as volumes of "sand" and "fine" sediment, and we combined these values to get the total suspended sediment discharge. We computed the suspended sediment concentration (SSC) in units of milligrams per liter (mg/L) using the equation:

$$\mathrm{SSC}\left(\frac{\mathrm{mg}}{\mathrm{L}}\right) = \frac{\mathrm{Q_s}\left(\frac{\mathrm{kg}}{\mathrm{s}}\right)}{\mathrm{Q}\left(\frac{\mathrm{m^3}}{\mathrm{s}}\right)} \mathrm{x}\, \frac{\mathrm{m^3}}{1000\ \mathrm{L}} \mathrm{x}\, \frac{1000\ \mathrm{g}}{1\ \mathrm{kg}} \mathrm{x}\, \frac{1000\ \mathrm{mg}}{\mathrm{g}} \qquad [1]$$

We only used data points on days where both a Q and Q_s measurement were collected (there was not a Q measurement for every Q_s measurement and vice versa). A summary of the SSC data is shown in Table 1. We analyzed the SSC data for quality control and excluded SSC values which were anomalously high or low.

TABLE 1: Summary of in SSC data

Station Name	River	Start date	End date	No. SSC samples
Bahadurabad	Brahmaputra-Jamuna	4/1/1968	10/23/2018	577
Hardinge Bridge	Ganges-Padma	8/3/1997	8/28/2019	143
Baruria	Padma	1/4/1991	6/27/2019	704
Mawa	Padma	8/4/2004	9/25/2019	181

3.2. Satellite data

Satellite data was downloaded and processed using Google Earth Engine (GEE), a cloud-based remote sensing platform (Gorelick et al., 2017). We used GEE for its multiple advantages including high-performance cloud-computing, free availability, and convenient user-interface capabilities. In GEE, Google's cloud infrastructure powers all data processing, stores all satellite datasets and data outputs, and immediately displays processed data on an interactive map. Users can export data in various file formats. GEE and all the datasets it contains are freely available for non-commercial use. GEE programming is done in Javascript, however customized applications can readily be developed and deployed so that non-programmers can easily operate them with a simple graphical user interface.

BROSS integrates data from multiple satellites, which are: Landsat 5 (TM), 7 (ETM+), and 8 (OLI); Sentinel-2; and MODIS (MOD09GA). Each of these satellites provide data in the visible (red, green, blue) and NIR wavelengths. However, the band wavelength ranges vary between satellites. These satellites also have different spatial resolution, temporal resolution, and temporal availability, as presented in Table 2. Although each Landsat satellite has a 16-day revisit interval, there is an 8-day offset between any two satellites that have overlapping operational periods. Landsat 7 has limited availability since 2003, when a failure of the Scan Line Corrector occurred (Chander et al., 2009). The calibration of Landsat 8 is significantly improved compared to Landsat 5 and 7 (Mishra et al., 2016).

TABLE 2: Satellite data used in BROSS

Satellite	Spatial Resolution	Temporal Resolution	Date Range	Band Ranges (nm)			
				Blue	Green	Red	NIR
Landsat 5 (TM)	30 m	16 days	1/1/1984-5/5/2012	441-514	519-601	631-692	772-898
Landsat 7 (ETM+)	30 m	16 days	4/15/1999- Present	441-514	519-601	631-692	772-898
Landsat 8 (OLI)	30 m	16 days	2/11/2013- Present	452-512	533-590	636-673	851-879
Sentinel-2	10 m	5 days	2017- Present	426-558	523-595	634-696	727-939
MODIS	500 m	1 day	2000- Present	459-479	545-565	620-670	841-876

Because of the differences between the band wavelength ranges and spatial resolutions of the satellites, separate regression and ANN models needed to be developed. We developed separate models for three distinct satellite groups:

1. Landsat 5 and 7: These have the same spatial resolution and nearly identical band ranges (except for a ~1 μm difference in the NIR [band 4] and shortwave infrared [band 7] ranges).
2. Landsat 8 and Sentinel-2: Although different, the data were corrected for differences so that they could be combined using algorithms developed by Zhang et al. (2018). There was also an insufficient number of Sentinel-2 data points to develop a reliable algorithm for this satellite alone.
3. MODIS

We used data satellite data with the highest quality rating for Landsat satellites (Tier 1), however this tiered rating was not an option for the other satellites. We used surface reflectance products from GEE that had already been atmospherically corrected. Although the Sentinel-2 satellite was launched in 2014, the surface reflectance records are not available in GEE until 2017. Surface water pixels were mapped for Landsat and Sentinel-2 by applying the Dynamic Surface Water Extent algorithm (Jones, 2015). For MODIS, surface water pixels were mapped used the index ranges for permanent water determined for Bangladesh rivers by Kwak et al. (2013).

Pixels with clouds and cloud shadows (except for Sentinel-2 for cloud shadows) were masked out of scenes to the extent feasible by combining multiple methods. One method was using the quality assessment (QA) bands of the surface reflectance datasets. Each dataset has QA bands for clouds, and the Landsat and MODIS datasets also have QA bands for cloud shadows. We also masked out pixels for which the sum of the red and blue bands was above a threshold (0.4 for Landsat, 0.6 for Sentinel-2, 0.9 for MODIS). Each threshold was determined through manual calibration. In addition, pixels were masked if any surface reflectance band (red, blue, green, or

NIR) was greater than 0.4. These methods for masking out clouds and cloud shadows are not perfect and that cloud impacts remain a limitation of BROSS, particularly in the wet season.

For calibrating the SSC models, we collected red, blue, green, and NIR data spatially-averaged over a stream reach roughly three times as long as the stream width at each in situ monitoring point (Figure 1). We retained samples with at least 30% of pixels classified as free of clouds and cloud shadows over the reach.

4. Calibration

We explored options for selecting/combining satellite data to calibrate the empirical relationship between SSC and surface reflectance. We used options which had the strongest performance and made physical sense. The options we explored and selected are the following:

- **In situ monitoring stations:** These were tested individually and combined. **We ultimately decided to use data from the Baruria and Mawa monitoring stations.** These stations are along the Padma river (Figure 1) and therefore represent sediment properties of both upstream mainstem rivers. As we learned from BWDB, data from Baruria is most reliable. However, the Baruria dataset alone was small, so we added data from Mawa. Including data from Bahadurabad and Hardinge Bridge weakened the results, likely because the in situ and satellite data for these points was lower quality.
- **Satellites:** These were tested individually (e.g., MODIS) and combined (e.g., all Landsat and Sentinel-2 combined). **We ultimately decided to calibrate separately for three groups: (1) Landsat 8 and Sentinel-2; (2) Landsat 5 and 7; and (3) MODIS**. These groupings are discussed above (Section 3.2).
- **Satellite data inputs:** These were tested using single surface reflectance bands (red, green, blue, NIR), band ratios (red/green, red/blue, red/NIR, green/NIR), and other band combinations that have been found to be significant in literature ((red+green)/2, red/green + NIR, Peterson et al. 2018). **The inputs varied between regression and ANN and for each satellite group** and are further described below.
- **Data overlap:** These were tested with in situ and satellite data collected on the same day, within ±1 day, and within ±2 days. **We ultimately decided to calibrate with in situ and**

satellite data collected within ±2 days (similar to Market et al., 2018 and Beveridge et al., 2020)

- **Seasons:** These were tested for seasons individually (e.g., wet, dry) and combined. **We ultimately decided to calibrate with the seasons combined.**
- **SSC ranges:** These were tested for SSC ranges separately (e.g., low: ≤100 mg/L and high: >100 mg/L) and combined. **We ultimately decided to calibrate with the SSC ranges combined.**

4.1 Regression

We tested both the SSC and reflectance values in linear and exponential forms with exponential, linear, and 2nd order models. Values in linear form and in exponential models were the strongest performing. We randomly divided the dataset as 70% calibration points and 30% testing points. This random division was conducted 30 times for each satellite group. We selected the highest performing empirical equation and calibration/testing grouping for the 30 iterations. The code for this calibration is found at https://github.com/cbev/bross/blob/master/Sediment_Regression.ipynb.

4.2 ANN

We used the Keras package (https://keras.io/) in Python to develop and implement the ANN model. For all models, we used:

- Feedforward model architecture
- Sequential models, which are linear stacks of layers
- Densely connected neural network layers
- Rectified linear unit activation functions, which are ideal for model non-linearity
- Scaled input data to have a zero mean and unit variance
- Optimization conducted using “adam” algorithm
- Optimization based on the mean-square-error metric

The top performing ANN model architecture and inputs slightly varied for each model, as shown in Table 3. We randomly divided the dataset as 70% calibration points and 30% testing points.

This random division was conducted 20 times for each satellite group. We selected the highest performing ANN model for the 20 iterations. The codes for the calibrations are found at: https://github.com/cbev/bross/blob/master/Calibrate_ANN_Landsat8Sentinel2.ipynb, https://github.com/cbev/bross/blob/master/SedimentANN_L5L7.ipynb, https://github.com/cbev/bross/blob/master/SedimentANN_MOD.ipynb

TABLE 3: Summary of ANN models' architecture

Satellite(s)	Inputs	# of layers	# of units per layer	batch size	# epochs
Landsat 8 & Sentinel-2	red, green, blue, NIR, red/blue, red/green, red/NIR, red+green+blue, (red+green)/2, red/green+NIR, month, satellite	10	128, 64, 64, 32, 16, 16, 8, 8, 4, 1	10	200
Landsat 5 & Landsat 7	red, green, blue, NIR, red/blue, red/green, red/NIR, red+green+blue, (red+green)/2, red/green+NIR, month	6	128, 64, 32, 8, 4, 1	14	300
MODIS	red, green, blue, NIR, red/blue, red/green, red/NIR, (red+green)/2, red/green+NIR, month	7	128, 64, 64, 32, 8, 4, 1	10	220

5. Results

Plots comparing the in situ SSC observations with regression and ANN models (training and testing data) are shown in Figure 2. The performance metrics for the regression and ANN models testing datasets (e.g., 30% of data that was used to test, not train, the models) are shown in Table 4. The five metrics we used to assess the models are:

- Root mean square error (RMSE): This is a common and strong hydrologic modeling metric that shows the prediction error in the terms of the variable being calculated (Ritter and Munoz-Carpena, 2013), which in our case is SSC (mg/L). RMSE is defined as

$$RMSE = \sqrt{\frac{\sum_{i=1}^{N}(O_i - P_i)^2}{N}} \qquad [2]$$

  where O is the observations, P is model predictions, and N is the number of samples. The RMSE range is 0 to ∞, and the lower the RMSE the stronger the results are.

- Coefficient of determination (r^2): This is another common hydrologic modeling metric which quantifies the degree of collinearity between the observed and predicted SSC. It is defined as

$$r^2 = \left(\frac{\sum_{i=1}^{N}(O_i-\bar{O})\,(P_i-\bar{P})}{\sqrt{\sum_{i=1}^{N}(O_i-\bar{O})^2}\sqrt{\sum_{i=1}^{N}(P_i-\bar{P})^2}} \right)^2 \qquad [3]$$

The r^2 range is 0 to 1, where 0 means no correlation and 1 means a perfect fit.

- Anomaly: This is the average deviation between the predicted SSC and the respective long-term observed monthly mean SSC. It is defined as

$$\text{Anomaly} = \frac{\sum_{i=1}^{N}(P_i-M_i)}{N} \qquad [4]$$

where *M* is the long-term observed monthly mean SSC (i.e., based all al *O*) for the same month that each *P* is made. It is the same units as the variable being measured (SSC, mg/L). It ranges from to -∞ to to ∞ and results are stronger when they are closer to 0. A positive anomaly means the prediction is higher than the observed monthly mean and a negative anomaly means the prediction is lower than the observed monthly mean.

- Anomaly correlation coefficient (ACC): This metric is common in weather forecasting and tests the correlation between the anomalies (see [4]) of observation and predictions. It is defined as

$$\text{ACC} = \frac{\sum_{i=1}^{N}\frac{\overline{(P_i-M_i)(O_i-M_i)}}{\sqrt{\overline{(P_i-M_i)^2}\;\overline{(O_i-M_i)^2}}}}{N} \qquad [5]$$

The ACC range is -1 to 1, where 1 means perfect coincidence between the anomalies of the prediction and observations, -1 means that the anomalies of the prediction and observations are perfectly reversed, and 0 means no correlation (Japanese Meteorological Agency, 2013)

- Spearman r (r_s): This is a nonparametric measurement based on the rank of data and is defined as

$$r_s = 1 - \frac{6\sum_{i=1}^{N}[R(O_i)-R(P_i)]^2}{N^3-N} \qquad [6]$$

where *R(Oi)* and *R(Pi)* are *O* and *P* of corresponding ranks. Like ACC, the r_S range is -1 to 1, where 1 means perfect correlation of the prediction and observations, -1 means that the correlation is perfectly reversed, and 0 means no correlation (Hamed, 2016). Because r_s is based on ranked data, it captures the non-linearity of data.

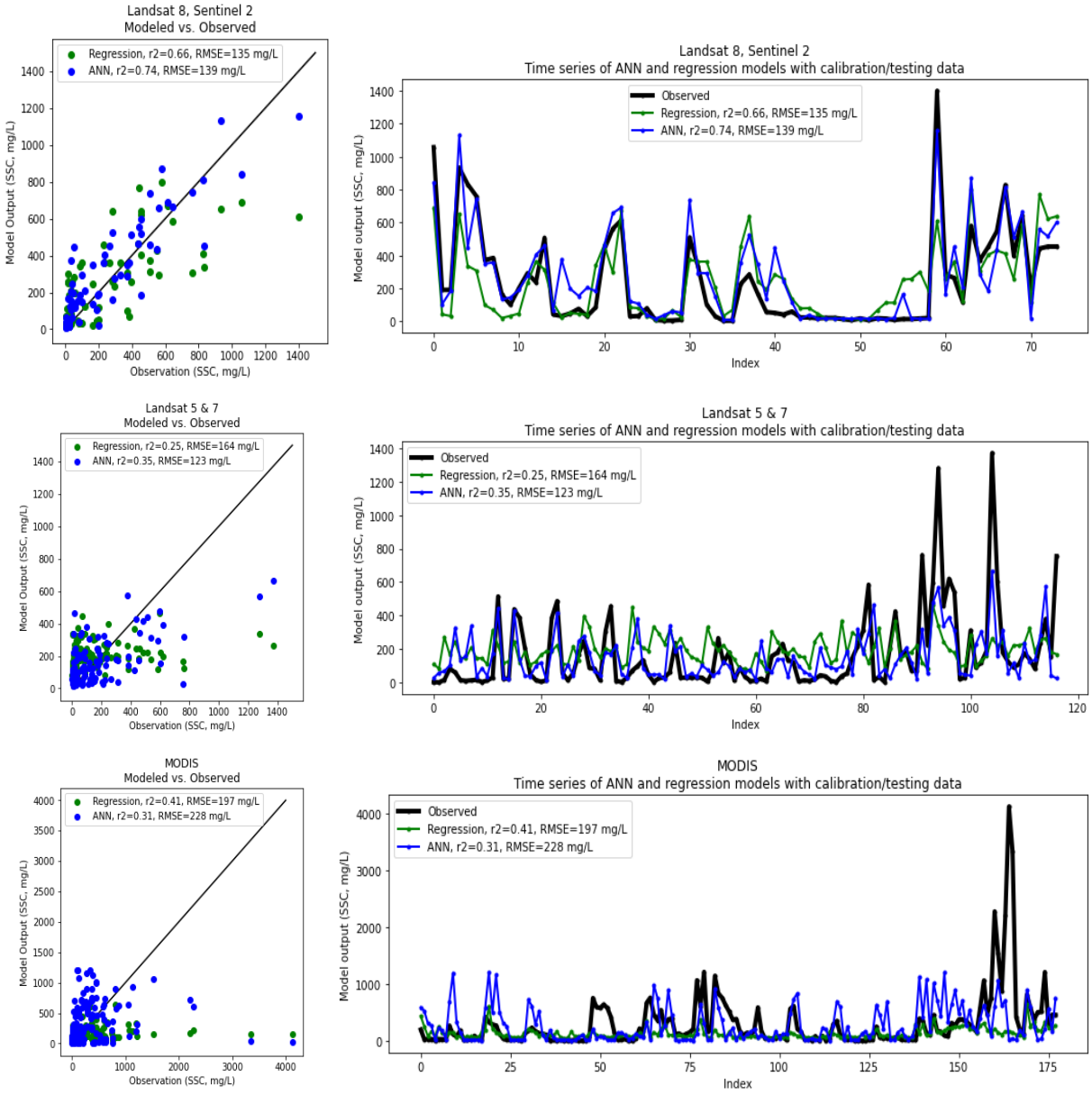

FIGURE 2: Comparison of SSC in situ observations with Regression and ANN models.

TABLE 4: Summary of ANN and Regression model performance. *Stronger result for each satellite group is indicated in* ***bold***

RMSE	ANN	Regression
Landsat 8 + Sentinel 2	139 mg/L	**134 mg/L**
Landsat 5 + Landsat 7	**123 mg/L**	165 mg/L
MODIS	228 mg/L	**202 mg/L**

r^2	ANN	Regression
Landsat 8 + Sentinel 2	**0.74**	0.71
Landsat 5 + Landsat 7	**0.35**	0.22
MODIS	0.31	**0.40**

Anomalies	ANN	Regression
Landsat 8 + Sentinel 2	**-102 mg/L**	-130 mg/L
Landsat 5 + Landsat 7	**-236 mg/L**	-386 mg/L
MODIS	**-70.2 mg/L**	-278 mg/L

ACC	ANN	Regression
Landsat 8 + Sentinel 2	**0.86**	0.83
Landsat 5 + Landsat 7	**0.93**	0.89
MODIS	0.52	**0.61**

r_s	ANN	Regression
Landsat 8 + Sentinel 2	**0.88**	0.81
Landsat 5 + Landsat 7	**0.60**	0.46
MODIS	**0.64**	**0.64**

As seen in Table 4 and Figure 2, the overall the performance of the ANN models is generally stronger than the regression models for the Landsat 5 + 7 and Landsat 8+ Sentinel-2 groups. For MODIS, the regression metrics are generally stronger or equal. This is likely because MODIS satellite data has larger spatial resolution and reduced ability to filter clouds and landscape. With the lower quality of MODIS data, the ability of ANN to capture patterns is poor and the more general trend captured by regression is stronger. It is also clear that the Landsat 8+Sentinel-2 models are generally stronger than Landsat 5+ Landsat 7 which is likely because of the improved calibration of Landsat 8 compared to previous Landsat satellites (Mishra et al., 2016) as well as the higher resolution of Sentinel-2.

Overall, the results are acceptable although not as strong as results in other studies (e.g., Peterson et al. (2018) ANN testing performance was r^2 of 0.78-0.81 and RMSE of 71.7 mg/L-93.1 mg/L). There may be various reasons for this such as the complexity of the river system and the quality

and consistency of the in situ and satellite data. The limitations and uncertainties are further discussed in section 6.

6. Limitations and uncertainty

There are notable limitations and sources of uncertainty in the regression and ANN approaches used for estimating SSC from satellite data in Bangaldesh rivers. River sediment properties (e.g., color, mineralogy, grain size distribution) and the presence of other suspended or dissolved material (e.g., chlorophyll, carotenoids) are known to vary throughout the river system spatially and temporally (e.g., Delft Hydraulics & DHI, 1996). These complexities in river sediment and surface reflectance can limit the spatial and temporal applicability of the regression and ANN models (Pavelsky et al., 2009). Furthermore, the regression and ANN models were based only on data from the Baruria and Mawa monitoring locations, which are along the Padma river. Therefore, the system does not explicitly account for differences in sediment properties along the Ganges-Padma and Brahmaputra-Jamuna rivers.

Another limitation comes from the penetration depth of satellite sensors for surface reflectance of water, which is the top ~1-2 meters. When the river bottom is shallower than the sensor penetration depth, it will scatter the remote sensing reflectance (Volpe et al., 2011). When the river bottom is deeper than the sensor penetration depth, the SSC measured in the surface layer may significantly differ from the depth-integrated SSC. This latter case is likely to occur at high discharges, when bedload and coarser sediment in the lower water column may be a higher proportion of the total load. Thus, SSC predicted from remote sensing cannot be directly used for depth-integrated SSC analyses and modeling. Furthermore, it is not possible to differentiate if increases in SSC prediction are resulting from suspended sediment increases in the entire water column, mixing between the lower and upper water columns (Markert et al., 2018), or from shallow channel depths. This poses a significant challenge in the complex, dynamic rivers of Bangladesh where the river depth is frequently changing spatially and temporally.

The temporal extent and frequency of remote sensing imagery can also limit its capacity to monitor SSC (e.g., 8- or 16- day revist interval for Landsat; Sentinel-2 available since 2017). Imagery availability and quality may be limited due to cloud cover. Cloud cover is prevalent in Bangladesh due to its monsoonal hydroclimatology. Hence, it is generally appropriate to rely on remote sensing for monitoring background seasonal SSC rather than isolated events (Wackerman

et al., 2017; Beveridge et al., 2020). Seasonal SSC from dry, non-cloudy seasons is more reliable than that from wet, cloudy seasons.

The spatial resolution of remote sensing imagery (e.g., 30m for Landsat) can also limit the use of satellite remote sensing for sediment. The stream locations where SSC can be monitored must have river channels wide enough that there are sufficient remote sensing pixels of water that do not mix with the river banks. Narrow channel widths, particularly in braided reaches along the Brahmaputra-Jamuna River, may have significant limitations because of this. The spatial resolution is a notable limitation for MODIS imagery (500m resolution) and a primary reason that the performance of the MODIS models is relatively low. Although the BROSS algorithms are set up to filter out land surfaces, they are not perfect.

There are also inherent limitations in using regression and ANN techniques. The models are both empirically-based and therefore may not appropriately account for physical changes in river sediment properties. The models are typically unable to extrapolate beyond the range of data used for training (Maier and Dandy, 2000; Flood and Kartam, 1994; Minns and Hall, 1996). Therefore, the models are less reliable at capturing rare, peak SSC occurrences which may be of significant interest.

A primary interest that BWDB has in using BROSS is to improve the prediction and characterization of erosion and accretion patterns throughout the river system. However, there is not a simple or clear relationship between SSC patterns and erosion/accretion patterns. Therefore, caution should be used when using the satellite monitoring data to make predictions about the complex river behavior.

7. Future work and conclusion

The following steps can be taken in future work to improve BROSS and how it can support BWDB sediment management:

- Continue to explore if and how the regression and ANN models can be improved.
- Continue to collect high-quality in situ SSC samples and use this data to improve the calibration of the ANN and regression models. This in situ data would need to be collected on the same day that a satellite is collecting data.

- Develop separate algorithms (regression and/or ANN) for the Ganges-Padma, Brahmaptura-Jamuna, and Padma river branches when there is an adequate amount of additional calibration data
- Investigate if and how satellite data predictions can help to understand the river sediment concentration profiles (vertical and lateral), possibly by combining with other data, models, and theories
- Investigate if and how SSC relates to and may help in the prediction of riverbank erosion and channel accretion.

The Bangladesh river system is one of the most complicated in the world when it comes to river sediment challenges. Thus, findings from this work will not only benefit BWDB and the people of Bangladesh; they can give meaningful insights to scientific knowledge and sediment monitoring and management strategies for global rivers.

8. References

Beveridge, C. and Ahmad, S.K., 2020. BROSS User Manual- SASWE System. Unpublished User Manual [Draft]. https://github.com/cbev/bross/blob/master/manual_user_SASWE.pdf

Beveridge, C., 2020. BROSS User Manual- Google Earth Engine. Unpublished User Manual [Draft]. https://github.com/cbev/bross/blob/master/manual_user_GEE.pdf

Beveridge, C., Bonnema, M., & Hossain, F., 2020. Impacts of dam development and landscape changes on suspended sediment concentrations in the Mekong River Basin's '3S' tributaries: a satellite remote sensing perspective. Journal of Hydrologic Engineering.

Beveridge, C., Ahmad, S. K., Biswas, N., & Hossain, F. (In preparation). Stakeholder-driven development of a cloud-based, satellite remote sensing tool to monitor suspended sediment concentrations in major Bangladesh rivers. Environmental Modelling and Software.

Chander, G., Markham, L., Halder, D.L., 2009. Summary of current radiometric calibration coefficients for Landsat MSS, TM, ETM+, and EO-1 ALI sensors. Remote Sens. Environ. 113, 893–903.

Delft Hydraulics & Danish Hydraulic Institute (DHI), 1996. Mineralogical and physical properties of river sediments. Special Report No. 14, River Survey Project (FAP 24), Prepared for Water Resources Planning Organization (WARPO), Dhaka, Bangladesh.

Flood, I., Kartam, N., 1994. Neural networks in civil engineering. I: Principles and understanding. Journal of Computing in Civil Engineering 8 (2), 131–148.

Gholizadeh, M.H., Melesse, A.M., Reddi, L., 2016. A comprehensive review on water quality parameters estimation using remote sensing techniques. Sensors (Switzerland) 16. https://doi.org/10.3390/s16081298

Gorelick, N., Hancher, M., Dixon, M., Ilyushchenko, S., Thau, D., & Moore, R. (2017). Google Earth Engine: Planetary-scale geospatial analysis for everyone. Remote Sensing of Environment.

Hamed, K. H., 2016. The distribution of Spearman's rho trend statistic for persistent hydrologic data, Hydrological Sciences Journal, 61:1, 214-223, DOI: 10.1080/02626667.2014.968573

Islam, M. R., Yamaguchi, Y., Ogawa, K., 2001. Suspended sediment in the Ganges and Brahmaputra rivers in Bangladesh: Observation from TM and AVHRR data, Hydrol. Processes, 15, 493 – 509, doi:10.1002/hyp.165.

Japanese Meteorological Agency, 2013. Appendix A- Verification Indices. Outline of the Operational Numerical Water Prediction at the Japan Meteorological Agency. https://www.jma.go.jp/jma/jma-eng/jma-center/nwp/outline2013-nwp/pdf/outline2013_Appendix_A.pdf

Jones, J.W., 2015. Efficient wetland surface water detection and monitoring via landsat: Comparison with in situ data from the everglades depth estimation network. Remote Sens. 7, 12503–12538. https://doi.org/10.3390/rs7091250

Kwak, Y., Arifuzzanman, B., Iwami, Y., 2015. Prompt Proxy Mapping of Flood Damaged Rice Fields Using MODIS-Derived Indices. Remote Sensing 7, 15969–15988.

Loy, J., 2019. Neural network projects with Python: The ultimate guide to using Python to explore the true power of neural networks through six projects.

Maier, H.R., Dandy, G.C., 2000. Neural networks for the prediction and forecasting of water resources variables: a review of modelling issues and applications. Environ. Model. & Softw. 15 (1), 101–124.

Markert, K.N., Schmidt, C.M., Griffin, R.E., Flores, A.I., Poortinga, A., Saah, D.S., Muench, R.E., Clinton, N.E., Chishtie, F., Kityuttachai, K., Someth, P., Anderson, E.R., Aekakkararungroj, A., Ganz, D.J., 2018. Historical and operational monitoring of surface sediments in the Lower Mekong Basin using Landsat and Google Earth Engine cloud computing. Remote Sens. 10, 1–19. https://doi.org/10.3390/rs10060909

Minns, A.W., Hall, M.J., 1996. Artificial neural networks as rainfall–runoff models. Hydrological Sciences Journal 41 (3), 399–417.

Mishra, N., Helder, D., Barsi, J., Markham, B., 2016. Continuous calibration improvement in solar reflective bands: Landsat 5 through Landsat 8. Remote Sens. Environ. 185, 7-15.

Pavelsky, T.M., Smith, L.C., 2009. Remote sensing of suspended sediment concentration, flow velocity, and lake recharge in the Peace-Athabasca Delta, Canada. Water Resour. Res. 45, 1–16. https://doi.org/10.1029/2008WR007424

Peterson, K.T., Sagan, V., Sidike, P., Cox, A.L., Martinez, M. 2018. Suspended Sediment Concentration Estimation from Landsat Imagery along the Lower Missouri and Middle Mississippi Rivers Using an Extreme Learning Machine. Remote Sens. 10, no. 10: 1503.

Ritchie, J.C., Cooper, C.M., Yongqing, J., 1987. Using landsat multispectral scanner data to estimate suspended sediments in Moon Lake, Mississippi. Remote Sens. Environ. 23, 65–81. https://doi.org/10.1016/0034-4257(87)90071-X

Ritchie, J.C., Zimba, P.V., Everitt, J.H., 2003. Remote sensing techniques to assess water quality. Photogramm. Eng. Remote Sens. 69, 695–704.

Sudheer, K.P., Chaubey, I., Garg, V., 2006. Lake water quality assessment from Landsat thematic mapper data using neural network: An approach to optimal band combination selection. J. Am. Water Resour. Assoc. 42, 1683–1695.

Volpe, V., Silvestri, S., Marani, M., 2011. Remote sensing retrieval of suspended sediment concentration in shallow waters. Remote Sens. Environ. 115, 44–54. https://doi.org/10.1016/j.rse.2010.07.013

Wackerman, C., Hayden, A., Jonik, J., 2017. Deriving spatial and temporal context for point measurements of suspended-sediment concentration using remote-sensing imagery in the Mekong Delta. Cont. Shelf Res. 147, 231–245. https://doi.org/10.1016/j.csr.2017.08.007

Yepez, S., Laraque, A., Martinez, J.M., De Sa, J., Carrera, J.M., Castellanos, B., Gallay, M., Lopez, J.L., 2018. Retrieval of suspended sediment concentrations using Landsat-8 OLI satellite images in the Orinoco River (Venezuela). Comptes Rendus - Geosci. 350, 20–30. https://doi.org/10.1016/j.crte.2017.08.004

Zhang, M., Dong, Q., Cui, T., Xue, C., Zhang, S., 2014. Suspended sediment monitoring and assessment for Yellow River estuary from Landsat TM and ETM+ imagery. Remote Sens. Environ. 146, 136–147. https://doi.org/10.1016/j.rse.2013.09.033

Zhang, H.K., Roy, D.P., Yan, L., Li, Z., Huang, H., Vermote, E., Skakun, S., Roger, J.C., 2018. Characterization of Sentinel-2A and Landsat-8 top of atmosphere, surface, and nadir BRDF adjusted reflectance and NDVI differences. Remote Sens. Environ. 215, 482–494.